Developmental Biology 332 (2009) 383–395

Contents lists available at ScienceDirect

Developmental Biology

journal homepage: www.elsevier.com/developmentalbiology

Lack of the mesodermal homeodomain protein MEOX1 disrupts sclerotome polarity and leads to a remodeling of the cranio-cervical joints of the axial skeleton

Susan Skuntz [a,1], Baljinder Mankoo [b,1], Minh-Thanh T. Nguyen [a,2], Elisabeth Hustert [c,3], Atsuo Nakayama [a,4], Elisabeth Tournier-Lasserve [a,5], Christopher V.E. Wright [d], Vassilis Pachnis [e], Kapil Bharti [a], Heinz Arnheiter [a,*]

[a] Mammalian Development Section, National Institute of Neurological Disorders and Stroke, National Institutes of Health, Bethesda, Maryland, USA
[b] King's College London, Randall Division of Cell and Molecular Biophysics, School of Biomedical and Health Sciences, New Hunt's House, London, SE1 1UL, UK
[c] Institute für Humangenetik und Anthropologie, Freiburg, Germany
[d] Vanderbilt University Medical Center Program in Developmental Biology, Vanderbilt University Medical Center, Nashville, Tennessee, USA
[e] Division of Molecular Neurobiology, National Institute for Medical Research, London NW7 1AA, UK

ARTICLE INFO

Article history:
Received for publication 6 March 2009
Revised 3 June 2009
Accepted 4 June 2009
Available online 9 June 2009

Keywords:
Cranio-cervical fusion
Vertebral fusion
Hemivertebrae
Tbx18
Uncx
Bapx1
Chromatin immunoprecipitation

ABSTRACT

Meox1 and *Meox2* are two related homeodomain transcription factor genes that together are essential for the development of all somite compartments. Here we show that mice homozygous for *Meox1* mutations alone have abnormalities that are restricted to the sclerotome and its derivatives. A prominent and consistent phenotype of these mutations is a remodeling of the cranio-cervical joints whose major feature is the assimilation of the atlas into the basioccipital bone so that the skull rests on the axis. These abnormalities can be traced back to changes in the relative rates of cell proliferation in the rostral and caudal sclerotome compartments, and they are associated with alterations in the expression of at least three transcription factor genes, *Tbx18*, *Uncx*, and *Bapx1*. As previously observed for *Bapx1*, MEOX1 protein occupies evolutionarily conserved promoter regions of *Tbx18* and *Uncx*, suggesting that *Meox1* regulates these genes at least in part directly. Hence, *Meox1* is part of a regulatory circuit that serves an essential, non-redundant function in the maintenance of rostro-caudal sclerotome polarity and axial skeleton formation.

Published by Elsevier Inc.

Introduction

A key feature in the establishment of the vertebrate body plan is the transient formation of somites which not only give rise to dermis and muscle but also to the axial skeleton. Somitogenesis follows a series of well-orchestrated processes that include polarization and spatially and temporally regular, reiterative segmentation of presomitic mesoderm, epithelialization, de-epithelialization, resegmentation, and cell differentiation (Gridley, 2006; Takahashi and Sato, 2008 for recent reviews). Among the many genes that regulate somitogenesis are two critical homeodomain transcription factors called *Meox1* and *Meox2*. *Meox1* was originally isolated from *Mus musculus* and in vertebrates is first expressed during gastrulation in early mesoderm and later in presomitic mesoderm, early somites, and throughout the dermomyotome and sclerotome, albeit at higher levels in the caudal sclerotome halves compared with the rostral halves (Candia et al., 1992; Candia and Wright, 1996). *Meox2* is not expressed in presomitic mesoderm but emerges along with *Meox1* in epithelial somites. Following the initiation of dorso-ventral somite differentiation, high-level *Meox2* expression is restricted to the sclerotome where it is again found at higher levels in caudal compared to rostral halves (Candia et al., 1992; Candia and Wright, 1996; Mankoo et al., 1999).

The importance of *Meox1* and *Meox2* in somitogenesis is evident from our previous analysis of mouse embryos with combined deficiencies in both genes (Mankoo et al., 2003). In such mutants, somites initially form but they are not organized as epithelial spheres, lack a basal lamina between them, have no recognizable dermomyotome, and show neither rostro-caudal polarization nor a sclerotomal segmentation. Consequently, newborns have profound deficiencies in skeletal muscles, lack ribs, and have a vertebra that particularly in its lumbar part is but a cartilaginous rod and lacks the customary tail vertebrae. This phenotype is the result of an alteration, reduction, or plain extinction of the expression of several somitic genes, including genes involved in early somitogenesis and differentiation of sclerotome and skeletal muscles. Hence, *Meox1*/*Meox2* together are needed for proper gene expression in *all* somitic compartments (Mankoo et al., 2003).

* Corresponding author. MDS, NINDS, NIH, Building 35, Room 2A-201, 35 Convent Drive MSC 3706, Bethesda, MD 20892-3706, USA. Fax: +1 301 480 2737.
E-mail address: ha3p@nih.gov (H. Arnheiter).
[1] These authors have contributed equally to the project.
[2] Present address: Department of Ophthalmology, College of Medicine, University of Cincinnati, Cincinnati, OH, USA.
[3] Present address: Scil Technology GmbH, Martinsried, Germany.
[4] Present address: Department of Embryology, Institute for Developmental Research, Aichi Human Service Center, Kasugai, Aichi, Japan.
[5] Present address: Université Paris Diderot – Paris 7, Paris, France.

0012-1606/$ – see front matter. Published by Elsevier Inc.
doi:10.1016/j.ydbio.2009.06.006

While the above results grossly delineate the functions of the two *Meox* genes in aggregate, they do not address the question of whether each may also have unique, non-redundant functions. In fact, previous results have shown that single *Meox2* null mutant mice lack specific muscles and have a generally reduced muscle mass but a normal axial skeleton, suggesting that *Meox1* substitutes for *Meox2* in the sclerotome but not the myotome (Mankoo et al., 1999). Here, we analyzed single *Meox1* null mutant mice and find that they have defects in axial skeleton but not muscle development, suggesting that *Meox2* compensates for the lack of *Meox1* in the myotome but not the sclerotome. The detailed analysis of the *Meox1*-associated phenotype shows major alterations in the cranio-cervical joints that were not anticipated from the analysis of the double mutants. These abnormalities are associated with transient imbalances in cell proliferation rates in rostral and caudal sclerotome compartments particularly in the rostral, developmentally older somites which give rise to the altered structures. Moreover, they correlate with alterations in the expression of three transcription factor genes, two of which, *Tbx18* and *Uncx* (formerly known as *Uncx4.1*) have previously been implicated in regulating rostro-caudal cell proliferation rates and maintenance of somite polarity (Bussen et al., 2004; Haenig and Kispert, 2004; Kraus et al., 2001; Tanaka and Tickle, 2004), and one of which, *Bapx1*, in regulating cell proliferation and chondrogenic differentiation of the ventro-medial sclerotome (Lettice et al., 1999; Tribioli and Lufkin, 1999; Akazawa et al. 2000). The results suggest that *Meox1* plays important, non-redundant roles in maintaining sclerotome polarity and, in particular, formation of the cranio-cervical joints.

Materials and methods

Generation, breeding, and genotyping of Meox1 mutant mice

Two lines of *Meox1* mutant mice, briefly described previously (Mankoo et al., 2003), were used in this study. One of them, designated *Meox1*$^{Tg(Mx1-TAX)2627Arnh}$ and here referred to as *Meox1*^{im}, carries a transgenic insertional mutation in *Meox1* and was kept on a mixed [C57BL/6;C3H/HeJ] background. The other, designated *Meox1*^{tm1Bmk} and here referred to as *Meox1*$^{-}$, carries a targeted allele of *Meox1* and was kept on a mixed [C57BL/6;129/Ola] background. A detailed molecular characterization of the mutant alleles is shown in Fig. S1 in the supplementary material. For genotyping, tail DNA was probed by Southern analysis or appropriate PCR reactions (for primer sequences, see Supplementary Table S1). Embryos (knockouts, transgenics, or compound heterozygotes) were genotyped by PCR reactions using embryonic membranes as source of genomic DNA.

Embryo harvest, in situ hybridizations, histological and skeletal preparations

Embryos were staged by counting somites or by determining the time elapsed between the morning a plug was found (E0.5) and harvest. For whole mount in situ hybridizations, riboprobes corresponded to position 314–576 of a *Meox1* cDNA or to cDNAs for *Meox2*, *Pax1*, *Pax9*, *Hoxd3*, *MyoD*, *Pax3*, *Foxc2* (B. Hogan), *Bapx1* (R. Hill), *Uncx* (B. Hogan), *EphA4*, *Dll3* (M. Kelley), *Tbx15* (G. Barsh), and *Tbx18* (A. Kispert). For embryonic cartilage analysis, 50-μm vibratome sections were prepared from alcian blue-stained embryos. Skeletal preparations of late gestation embryos and newborns were produced using a combination of alcian blue and alizarin red staining (Kessel et al., 1990). For immunocytochemistry (Nakayama et al., 1998), a rabbit antiserum directed against a MEOX1 fragment comprising residue 2–136 (Candia and Wright, 1996) and appropriate secondary antibodies were used on cryostat sections.

Chromatin immunoprecipitation (ChIP) assays

For ChIP assays, caudal tissue extending from the caudal boundary of the hindlimb bud to the end of the tail was harvested from 6 to 10 embryos (E10.5 or E11.5) and processed as described (Bharti et al., 2008), except that sonication was used for DNA shearing and ChIP IT Express Kit (Active Motif) was used for immunoprecipitation with the above mentioned rabbit anti-MEOX1 antiserum. Primers appropriate to amplify subregions in the *Tbx18* and *Uncx* upstream regulatory sequence (amplicons) were used as described in the text. Primer sequences are shown in Table S1 in the supplementary materials.

Cell counts, BrdU incorporation, TUNEL, and activated caspase-3 labeling

BrdU (50 μg/g body weight) was injected intraperitoneally into timed-pregnant mice. Twenty minutes later, mice were given another injection of 50 μg/g of BrdU and embryos were harvested 100 min later. Sagittal cryosections were prepared and labeled with mouse monoclonal antibody to BrdU (Becton Dickinson). TUNEL staining using terminal deoxynucleotidyl transferase, dUTP-biotin (Roche) and streptavidin–rhodamin (Jackson ImmunoResearch Laboratories) was done according to established protocols. Sections were also labeled with rabbit anti-cleaved caspase-3 antibody (Cell Signaling Technology) and appropriate biotinylated second antibody. Percent labeling is expressed as the mean or median of the fraction of labeled cells/total cells, counted separately for rostral and caudal somite compartments.

Results

Meox1 deficiency leads to a remodeling of the cranio-cervical joints and to vertebral abnormalities

As briefly described previously (Mankoo et al., 2003), we generated two lines of mice with distinct null mutations in *Meox1*. One of them, *Meox1*^{im}, carries a transgene array that was fortuitously inserted into intron 1 of *Meox1* and deleted 45,459 basepairs (bp) of genomic sequence that included exon 2, intron 2, exon 3 and flanking regions of *Meox1*. The other line, *Meox1*$^{-}$, carries a targeted allele that eliminates the transcriptional start site, exon 1, and 2276 bp of intron 1 of *Meox1* but leaves the remainder of the gene intact (Fig. S1 in the supplementary material). Both lines gave rise to homozygous embryos that lacked stable Meox1 transcripts and MEOX1 protein (Figs. 1A–F for a comparison between wild type and *Meox1*$^{im/im}$) and that did not show compensatory increases in the expression of *Meox2* (Figs. 1G–J, and data not shown). Hence, we conclude that both alleles are *Meox1* null alleles and that the associated phenotypes are due solely to the lack of *Meox1* and not to some other, unrecognized genomic alteration.

While *Meox1*^{im}/+ or *Meox1*$^{-}$/+ mice were phenotypically similar to wild-type mice, homozygous mutants showed a variable, though consistently shorter-than-normal stature and short, kinky tails (Fig. 2A). To analyze this phenotype in more detail, we stained late gestation embryos or newborn mice for cartilage and bone. Most consistently, the bones of the cranio-cervical joints of *Meox1*$^{im/im}$ or *Meox1*$^{-/-}$ homozygotes or *Meox1*$^{im/-}$ compound heterozygotes were remodeled in such a way that the anterior arch of the atlas (AAA) was assimilated into the basioccipital bone and the neural arches were partly deleted and/or fused with the exoccipitals and basioccipitals (Figs. 2B–G and Table S2 in the supplementary materials). In addition, the dens axis was deleted or projected upward through the AAA and was fused with the atlas in 16 of 17 homozygotes (Fig. 2D, arrow, and Table S2 in the supplementary materials). As a result of the entire remodeling of the cranio-cervical joints, the skull now rested on the axis rather than the atlas.

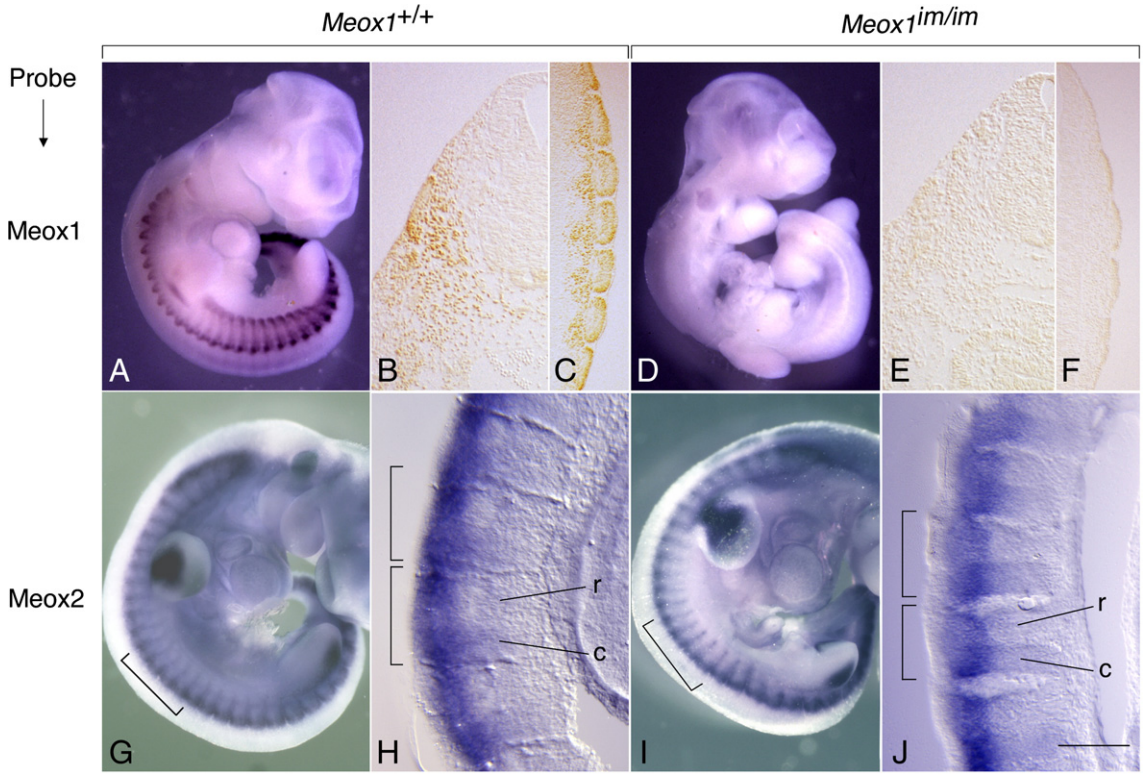

Fig. 1. *Meox1*^{im} is a null allele and does not lead to compensatory changes in *Meox2* expression. All embryos are at E10.5. (A, D) Whole mount in situ hybridizations for *Meox1*, using a Meox1 exon 1 probe whose genomic sequence is not deleted in *Meox1*^{im}. In contrast to wild-type (A), there is no signal in *Meox1*$^{im/im}$ (D). (B, C, E, F) MEOX1 protein expression in wild-type and *Meox1*$^{im/im}$ transverse (B, E) and coronal (C, F) sections, using a rabbit antiserum to an aminoterminal fragment of MEOX1 protein. (G–J) Similar *Meox2* expression in wild type (G, H) and *Meox1*$^{im/im}$ (I, J) embryos. (G, I) Whole mount in situ hybridizations. (H, J) Parasagittal vibratome sections. Brackets in (G) and (I) mark somites analyzed in (H) and (J), respectively. Brackets in (H) and (J) mark somite boundaries. r = rostral, c = caudal. Bar: 175 μm for B, E; 200 μm for C, F; 150 μm for H, J.

In addition to the abnormalities in the cranio-cervical joints, *Meox1* homozygotes also showed vertebral fusions and split vertebral ossification centers particularly in the lumbar and sacral regions, though the severity of this phenotype varied from animal to animal (Figs. 2K–N and Table S2 in the supplementary materials). Some homozygotes also had rib abnormalities characterized by small rib anlagen (not shown), lack of ribs (Fig. 2I, arrow), or rib bifurcations (Fig. 2J, arrow). All these skeletal malformations were mild, however, and so the homozygotes were fertile and had normal life spans.

Loss of Meox1 affects sclerotome patterning and leads to malformations in cartilaginous skeletal anlagen

To determine the underlying causes of the skeletal malformations, we performed a histological analysis of the mutant embryos. In contrast to somites of *Meox1*/*Meox2* double homozygotes (Mankoo et al., 2003), somites of E9.5 *Meox1*$^{im/im}$ (Figs. 3A, B) or *Meox1*$^{-/-}$ single mutants (not shown) were well defined and subcompartmentalized. At E10.5, sagittal sections through the midline (marked by the presence of the notochord, n), showed mesenchymal condensations in wild type (arrow in Fig. 3C) but not in *Meox1*$^{im/im}$ (Fig. 3D). In parasagittal sections, sclerotomal condensations were visible in both wild type and mutant but the alternation between rostral (r) and caudal (c) sclerotome halves was consistently less prominent in mutant (Figs. 3E, F). Moreover, the dorsal root ganglia, which were well separated in wild type, were partly fused in mutants (Figs. 3E, F, arrow). At E12.5, sclerotomal condensations were visible in the midlines of wild-type and mutant embryos, both in the cranio-cervical (Figs. 3G, H) and sacral regions (Figs. 3I, J), but compared with wild type (Figs. 3G, I), mutant condensations were less well defined and unequally spaced (Fig. 3J, arrows). A prominent difference was found in the position of the presumptive AAA which in mutant was not well defined and shifted towards the basioccipital anlage (Figs. 3G, H, arrow), presaging the subsequent fusion of the atlas and the basioccipital bone (see above, Figs. 2B–G).

To analyze the formation of cartilage, we stained sagittal and parasagittal sections of E13.5 and E14.5 embryos with alcian blue. In wild type (not shown) and *Meox1*^{im}/+ heterozygotes (Figs. 3K, O), the cartilage anlagen that eventually give rise to the basioccipital, exoccipital, atlas, the AAA, and axis were well formed. In *Meox1*$^{im/im}$ homozygotes, however, various cartilaginous anlagen were fused. For instance, the future AAA was shifted towards the base of the skull and fused with the basioccipital (arrow in Fig. 3L). One embryo showed fusions between the neural arches of the future axis and cervical vertebra 3 (C3) (Fig. 3P), and another a fusion between cervical vertebra C3 and C4 (C3/4) and a cartilaginous bridge between C7 and thoracic vertebra 1 (Th1) (Fig. 3Q). These fusions were not associated with defects in the nucleus pulposus of the intervertebral discs (Figs. 3K, L for E13.5 and high magnifications in M, N for E14.5). Taken together, the above results indicate that the deformations of the vertebral bones are foreshadowed in early sclerotomal deficiencies that subsequently affect the corresponding cartilaginous anlagen.

Meox1 mutations affect the expression of Bapx1, Uncx, and Tbx18

Some of the above mentioned phenotypes share similarities with those encountered with mutations in distinct somitic genes. Remodeling of the cranio-cervical joints, for instance, has been observed in mice with targeted mutations in the homeobox gene *Hoxd3*, alone or in combination with mutations in *Hoxa3* (Condie and Capecchi, 1993, 1994), and split vertebral ossification centers were seen with mutations in *Pax1*, *Foxc2*, and *Bapx1* (Iida et al., 1997; Winnier et al., 1997; Wilm et al., 1998; Lettice et al., 1999; Tribioli and Lufkin, 1999; Akazawa et al., 2000). Therefore, we investigated

whether the expression of these and related genes was altered in *Meox1* mutants. Compared with wild type, there were no consistent alterations in the levels or expression patterns of *Hoxd3*, *Pax1*, *Pax9* (Figs. 4A–H) and *Foxc2* (not shown) in *Meox1*$^{im/im}$ or *Meox1*$^{-/-}$ embryos. *Sox9*, a regulator of chondrogenesis, also remained normal in mutants (Fig. S2 in the supplementary material), and so did the expression of two regulators of myogenesis in the dermomyotome, *MyoD* and *Pax3* (Figs. 4I–L). Consistent with these latter observations, we did not see any histological defects in skeletal muscles during development or abnormalities that could indicate muscle defects in adults (not shown). Hence, we conclude that *Meox2* fully compensates for myotome development in *Meox1* mutants.

In contrast to the above mentioned genes, the expression of *Bapx1*, the mouse homolog of the *Drosophila* homeodomain gene *bagpipe*, was altered. This gene is normally expressed in overlap with *Meox1* and is essential for the development of the ventro-medial sclerotome (Lettice et al., 1999; Tribioli and Lufkin, 1999). Although at E9.5, there was no difference between control and mutant *Meox1*$^{-/-}$ embryos (data not shown), *Bapx1* expression was more diffuse and slightly reduced along the entire rostro-caudal axis at E10.5 (Figs. 5A, B), and even more so at E11.5 (Figs. 5C, D). Similar observations were made with *Meox1*$^{im/im}$ embryos (not shown). These findings were consistent with earlier results showing that the promoter of *Bapx1* contains MEOX1 binding sites and is regulated by MEOX1 in vitro (Rodrigo et al., 2004). Hence, *Meox1* appears to be required for the proper maintenance of *Bapx1* expression, though not for its initial onset. That *Bapx1* might indeed be part of the *Meox1* phenotype is further suggested by the fact that at E11.5, the reduction in *Bapx1* expression was particularly prominent in the rostral-most sclerotomes (Figs. 5C, D, arrows) which correspond to somites that give rise to the basioccipital, exoccipital, atlas, and axis bones where later the predominant skeletal pathology is found.

To explore why sclerotome polarization in *Meox1* mutants was not as clearly defined as in wild type (see, for instance, Figs. 3E, F), we specifically analyzed the expression of genes that are normally found selectively in the rostral or caudal somite compartment. *Uncx*, for instance, is normally expressed only in the caudal half of each somite and is required for the formation of derivatives of the caudal lateral sclerotome such as pedicles and proximal ribs (Leitges et al., 2000; Mansouri et al., 2000). In fact, initial whole mount in situ hybridizations at E9.5 showed a reduction in the number of *Uncx*-labeled rostral somites in *Meox1* mutants. Because rostral somites rapidly disperse, however, it is difficult to assign somite identities unequivocally during development, and so any comparison between wild type and mutant critically depends on the choice of appropriate axial landmarks. Of two proposed landmarks, namely the position and shape of the dorsal root ganglia (Sporle and Schughart, 1997) and the rostral boundary of the forelimb bud (Burke et al., 1995), the latter seems more appropriate for our comparison because in contrast to dorsal root ganglia, forelimb buds are not altered in the mutants. In fact, at E9.5 or E10.5, we usually find four recognizable somites rostral to the bud in both wild type and mutant.

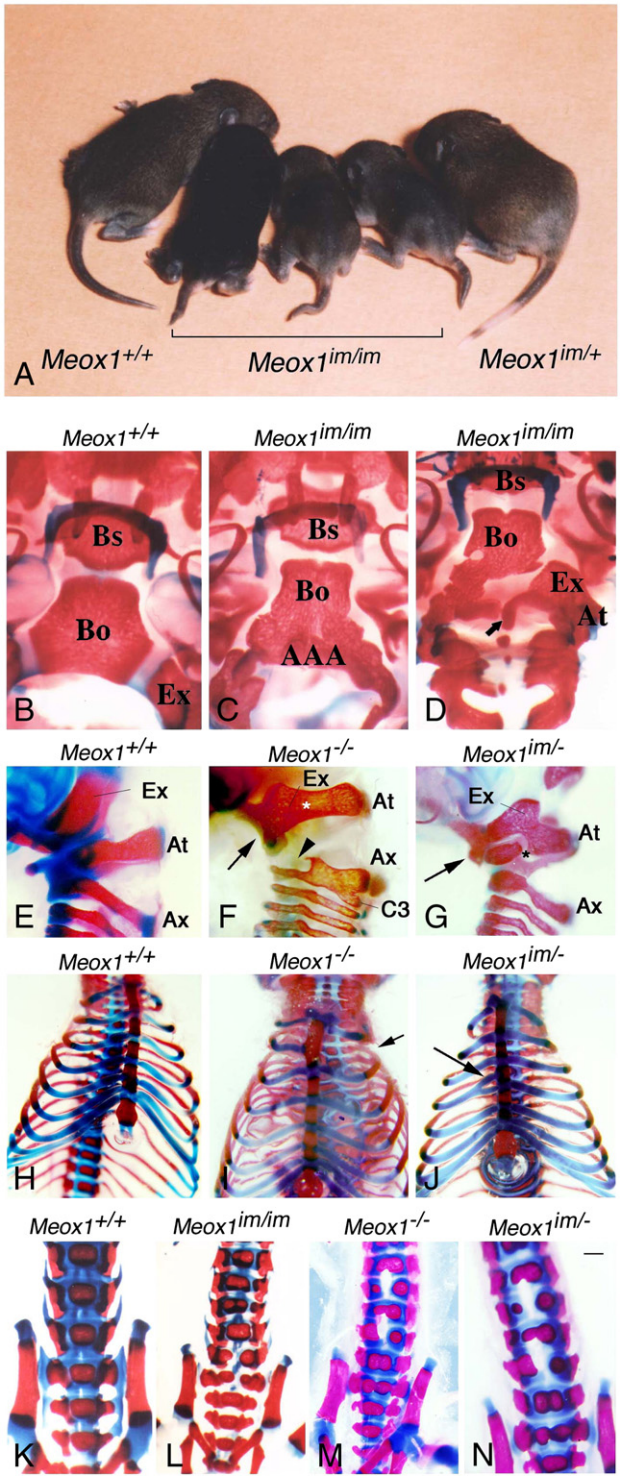

Fig. 2. Skeletal phenotype of *Meox1* mutant mice and their embryos. (A) Examples of mice homozygous for *Meox1*^{im}. Crosses between two *Meox1*^{im}/+ parents produce offspring that are smaller and have short, kinky tails. All mice with the tail phenotype are genotypically homozygous (*Meox1*$^{im/im}$), and all *Meox1*$^{im/im}$ homozygotes have the tail phenotype. Heterozygotes are phenotypically normal. Similar observations were made with the *Meox1*$^{-}$ allele (not shown). (B–N) Alcian blue (cartilage)/alizarine red (bone) skeletal preparations of wild-type and mutant late gestation embryos (B–D, K, L) and newborn mice (E–J, M, N). (B–G) remodeling of the cranio-cervical joints. (B) Wild type shows a clear separation of ossifications of basosphenoid (Bs), basioccipital (Bo), exoccipital (Ex) and atlas (not depicted). (C, D) In *Meox1*$^{im/im}$, the anterior arch of the atlas (AAA) is either incorporated into the Bo, as shown in (C), or the Bo is dysmorphic and the Ex fused with the atlas (At), as shown in (D). Arrow in (D) points to the dens axis that is fused with part of the Ex and At. (E–G) Lateral views of the cranio-cervical joint of wild type (E), *Meox1*$^{-/-}$ (F), and *Meox1*$^{im/-}$ compound heterozygotes (G). (F) Fusion (marked by arrow) of the ventral part of the AAA to the Bo and fusion (marked by white asterisk) of the At lateral masses to the Ex. Most of the ventral parts of the axis (Ax), including the dens axis, are deleted (arrowhead) while the caudal part of the remaining neural arch of the Ax, except for its spinous process, is fused to C3. (G) Fusion of part of the AAA with the Bo (arrow) and of the lateral mass of the At with the Ex. Note disconnection (marked by black asterisk) of the lateral mass of the At from the remainder of the At. (H–J) Low penetrance abnormalities of ribs. (H) Wild-type neonate. (I) *Meox1*$^{-/-}$ neonate. Note missing rib Th2 on the neonate's left side (arrow). (J) *Meox1*$^{im/-}$ neonate. Note bifurcation of distal end of rib Th4 on the neonate's right side (arrow). (K–N) Lumbar and sacral hemivertebrae in *Meox1* mutants. (K) Wild type control. Note normal ossification centers in the middle of the vertebral body. (L) *Meox1*$^{im/im}$. Note split of the middle ossification centers in lumbar and sacral region. A similar split in middle ossification centers is seen in *Meox1*$^{-/-}$ (M) and *Meox*$^{im/-}$ (N). Bar 1.0 mm for (K)–(N).

Uncx expression showed no differences between wild type and mutant embryos at E8.5 (not shown). At E9.5, *Uncx*-labeling was found in the caudal segments of the four rostral somites in both wild type and *Meox1* heterozygotes (Figs. 5E, G, rostral border of forelimb bud marked with white lines) but in *Meox1* homozygotes, only the caudal two of these four somites were clearly labeled (Figs. 5F, H). At E10.5, although all four somites were now labeled independent of the genotype, their staining was much weaker in the homozygotes (Figs. 5I, J for whole mounts, K, L for sagittal sections). This weakness in staining extended to the caudally adjacent somites (Figs. 5I, J). Hence, it appears that, reminiscent of the findings with *Bapx1*, *Uncx* expression is initially normal in *Meox1* homozygotes but then not properly maintained in the more rostral, developmentally older somites.

We then extended the analysis to genes expressed in the rostral somite compartment. *Dll3*, a member of the family of Notch ligands, is normally expressed in the presomitic mesoderm and in the rostral halves of newly formed somites but is quickly extinguished as somites mature (Dunwoodie et al., 1997). As shown in Figs. 6A, B, *Dll3* expression was similar in wild type and mutant. *EphA4*, which encodes an ephrin receptor tyrosine kinase, is normally expressed as a broad stripe at the rostral boundary of the presomitic mesoderm that marks the next somite to be formed and as a stripe in the rostral compartment of the most recently formed somite (Bergemann et al., 1995; Nakajima et al., 2006). The expression of *EphA4* also did not show a difference between wild type and mutant (Figs. 6C, D). These findings are consistent with the observation that *Uncx* expression was normal in the newly formed, caudal somites.

In contrast to *Dll3* and *EphA4*, *Tbx18*, a member of the large family of T-box containing transcription factor genes involved in mesoderm formation, is normally maintained in rostral somites at least until E10.5. As previously described (Kraus et al., 2001) and shown in Fig. 6E, in wild type, *Tbx18* was expressed at E8.5 in the rostral presomitic mesoderm (marked by white horizontal lines in Fig. 6E), in rostral somite compartments, and in the splanchnic mesoderm caudal and lateral to the heart tube (marked by arrowhead in Fig. 6E). Later, it was also found in the epicardium (Fig. 6F, arrowhead) and in limb buds. In *Meox1*$^{im/im}$ embryos, *Tbx18* expression was normal in E8.5 presomitic and splanchnic mesoderm but reduced in somites (Fig. 6J, white lines marking expression in presomitic and arrowhead in splanchnic mesoderm). The reduction in somitic expression continued through E10.5 (Figs. 6K–N) and beyond (not shown), arguing against a delayed onset of expression. Nevertheless, *Tbx18* expression was retained in other tissues where *Meox1* was not found at these stages, including in heart and limb buds (Figs. 6K, M, N). A close relative of *Tbx18*, *Tbx15*, shares similar expression patterns with *Tbx18* in limb buds and is highly expressed in unsegmented cranial mesenchyme but downregulated rapidly when mesenchymal cells condense into the skeletal primordia (Kuijper et al., 2005; Singh et al., 2005). Nevertheless, *Tbx15* expression, probed by whole mount in situ hybridization and analyzed on sagittal vibratome sections, did not show significant differences between wild type and mutant (Fig. S3 in the supplementary material) and so is unlikely to contribute to the *Meox1* phenotype.

MEOX1 binds the Tbx18 and Uncx promoters in vivo

The above results suggested that *Meox1* regulates the expression of *Tbx18*, *Uncx*, and *Bapx1*. In contrast to the promoter region of *Bapx1*, where MEOX1 binding sites have been described (Rodrigo et al., 2004), the promoter regions of *Tbx18* and *Uncx* have not so far been analyzed in detail and so it is unknown whether *Meox1* might regulate them directly or exclusively via other interposed regulators. To identify such binding sites, we concentrated on approximately 1 kbp of the respective upstream regulatory regions of both *Tbx18* and *Uncx* chiefly because interspecies comparisons revealed sequence conservation only in this region and not further upstream, and because the regions contained conserved motifs that might potentially serve as binding sites for MEOX1 (Rodrigo et al., 2004) (Figs. 7 and S4 in the supplementary materials). To determine whether *Meox1* can bind these motifs in vivo, we performed chromatin immunoprecipitation (ChIP) assays using caudal somites of E10.5 or E11.5 embryos as tissue source, the above mentioned rabbit anti-MEOX1 antiserum for immunoprecipitation, and primers designed to amplify the potential binding sites and their flanking regions as schematically shown on the left side of Figs. 7A, B. As shown in the middle panels of Fig. 7, ChIP assays yielded no specific bands for the *Tbx18* amplicons a, b, or c (Fig. 7A), or the *Uncx* amplicons a, b, and d (Fig. 7B). In contrast, the *Tbx18* amplicon d, covering the potential MEOX1 binding sites 7 and 8, and the *Uncx* amplicon c, covering the potential MEOX1 binding sites 4 and 5, gave MEOX1-specific bands. These positive amplicons were also found in *Meox1*^{im}/+ heterozygotes but not in *Meox1*$^{im/im}$ homozygotes, attesting to the specificity of the MEOX1 antiserum. Interestingly, the *Uncx* binding sites 4 and 5 are perfectly conserved from zebrafish to man, in contrast to the potential binding sites 1–3 and 6–8 which are less well-conserved. Also, the *Tbx18* binding site 8 is perfectly conserved from bird to mammal, in contrast to the other sites, and although zebrafish does not have a perfect match for binding site 8, it has a potential binding site at a similar location relative to the start site of transcription (Fig. S4 in the supplementary materials). Taken together, the results demonstrate that MEOX1 is indeed bound to specific sites in the respective promoters of *Tbx18* and *Uncx* in vivo and hence suggest that MEOX1 regulates the maintenance of these genes at least in part directly.

Lack of Meox1 affects somitic cell proliferation

The fact that *Tbx18* expression was reduced in *Meox1* mutant embryos prompted us to compare the consequences of a lack of *Meox1* with those of previously reported alterations of gene dose in *Tbx18* (Bussen et al., 2004). *Tbx18* null embryos show an increase in the number of cells in S-phase in the rostral sclerotome compartment, an increase in the number of apoptotic cells in the lateral rostral sclerotome compartment, and an expansion of derivatives of the caudal lateral sclerotome (pedicles, transverse processes, proximal ribs). Conversely, ectopic *Tbx18* expression in both somite halves leads to an expansion of the rostral at the expense of the caudal compartment, a reduction in the level of expression of genes normally found in the caudal halves, and a thinning of caudal somite derivatives, including pedicles and proximal ribs (Bussen et al., 2004).

In the light of these findings, we determined the rates of cell proliferation and cell death in rostral and caudal somite halves of *Meox1* mutants. For these assays, we focused on the occipital and cervical somites, reasoning that since the major phenotypes were found in derivatives of these somites, they might give us the best chance of finding relevant alterations. The percentage of cells in S-phase was determined from cryosections of BrdU-treated wild-type and *Meox1*$^{im/im}$ embryos, and the percentage of apoptotic cells by labeling corresponding sections by the TUNEL procedure or for activated caspase-3. Multiple sections from 2 to 4 embryos of each genotype were analyzed and the labeled cells were determined as a fraction of the total cells counted in the respective sclerotome compartments. Fig. 8A shows low-magnification representations of BrdU-labeled sagittal sections. Representative areas selected for counting are shown for the rostral-most recognizable somites. For E10.5, the first recognizable somite is usually referred to as occipital somite 4 (O4), but given the absence of an O4-specific marker applicable to these sections, we prefer to label it as somite 1. Based on the above mentioned criteria of the position of the forelimb bud as revealed from adjacent sections (not shown), wild-type somite 1

corresponds to mutant somite 1. The percentage of BrdU-positive cells in wild type was lower in rostral compared to caudal compartments ($p = 0.013$ for the values obtained from somite 1–7, Student's t-test), but no significant rostro-caudal difference was found in the corresponding mutant somites ($p = 0.5$). This latter result was due to an increase in the mean labeling index in the mutant rostral compartments paired with a decrease in the caudal compartments. These alterations, considered separately, did not reach statistical

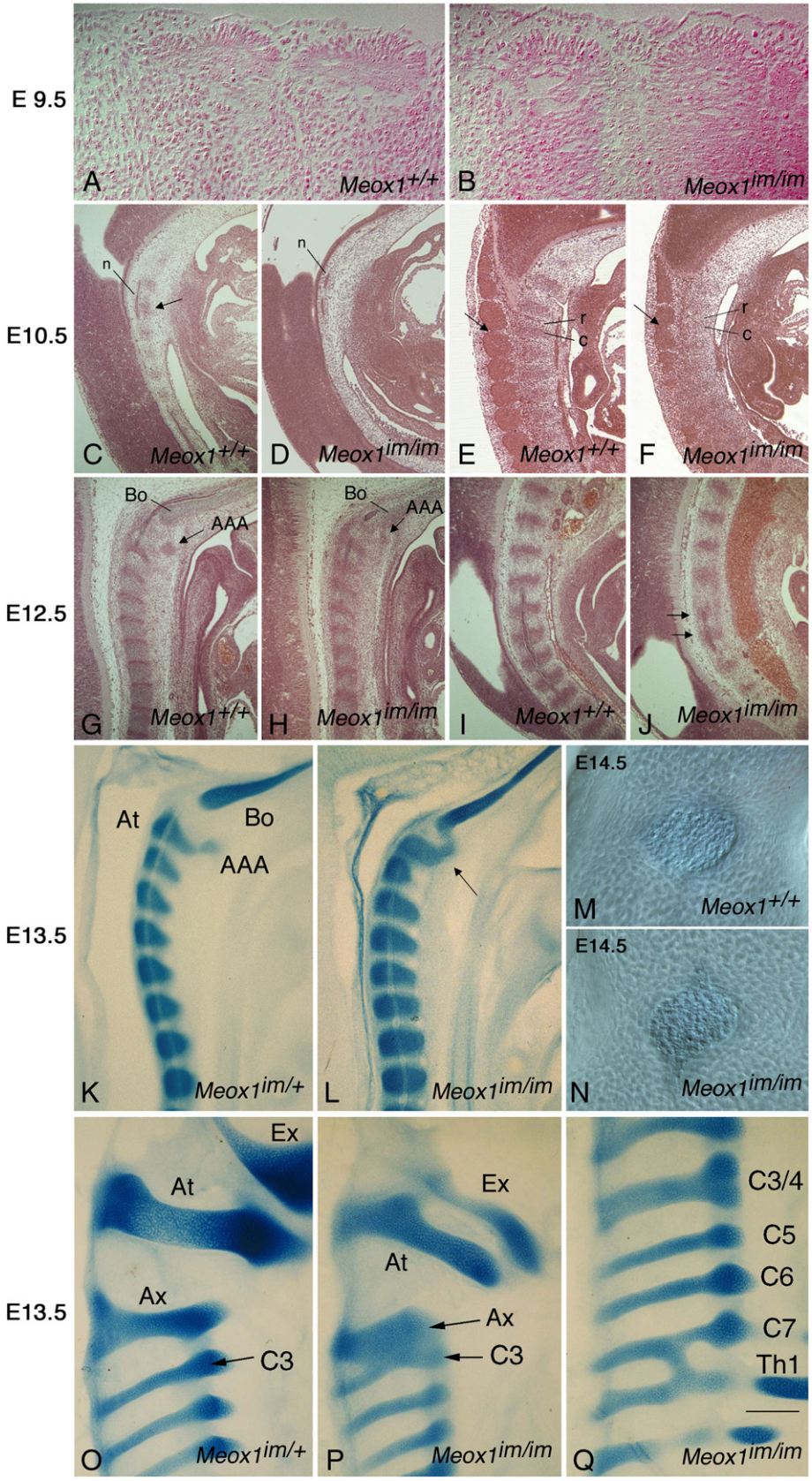

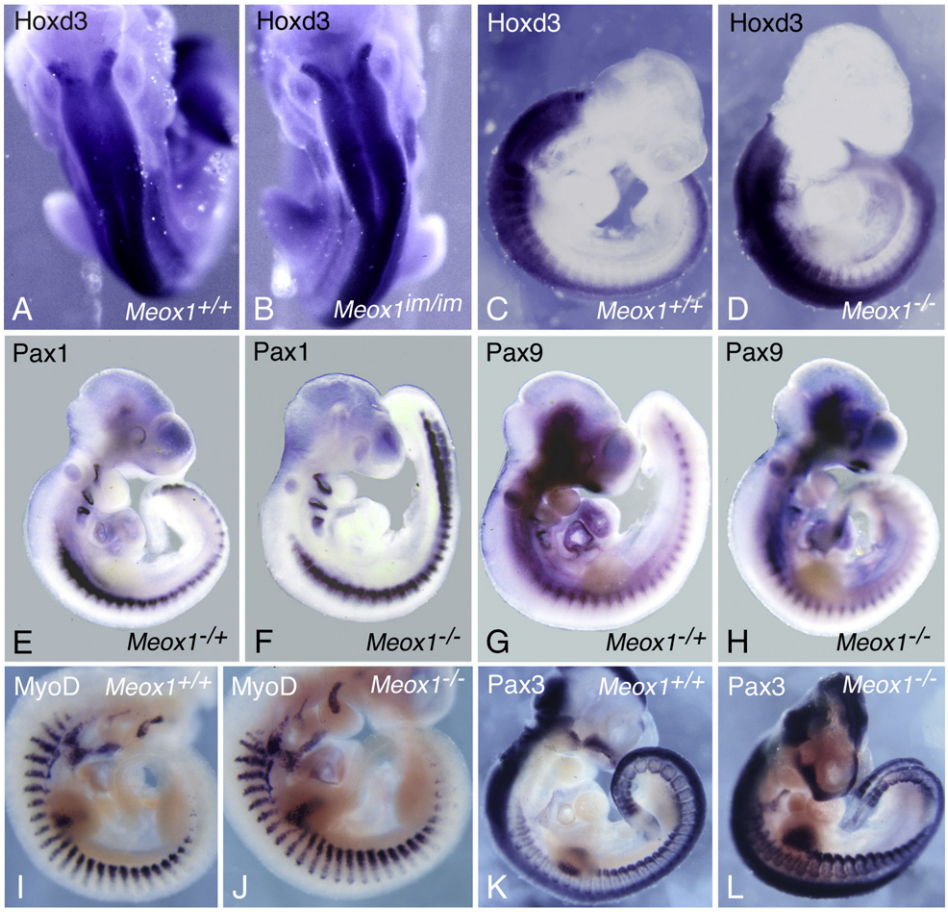

Fig. 4. Lack of *Meox1* does not alter the expression of a number of genes involved in skeletogenesis and myogenesis. Embryos of the indicated genotypes were harvested at E10.5 and processed for whole mount in situ hybridizations. (A, B) Wild-type and *Meox1*$^{im/im}$ embryos probed with Hoxd3, dorsal view. (C, D) Wild-type and *Meox1*$^{-/-}$ embryos probed with Hoxd3, lateral view. (E–L) Lateral views of embryos labeled with the indicated probes. No significant differences between wild type and mutant are seen.

significance, however, and were different from the results in *Tbx18* null mutants that showed increased BrdU incorporation in the rostal compartments only, without changes in the caudal compartments. Nevertheless, the end result, the loss of rostro-caudal intrasomitic differences in *Meox1* mutants, is consistent with the previous findings in E10.5 *Tbx18* null mutant embryos (Bussen et al., 2004).

At E12.5, the rostral boundary of the basioccipital derivative of somite O4 cannot be defined anatomically but we could clearly visualize the boundaries of cervical somite C1 because of its relationship to the condensation of the future AAA (arrows in sections of Fig. 8A). At this time point in development, overall BrdU incorporation rates were similar in wild type and mutant, and significant rostro-caudal differences were seen with both genotypes ($p<0.0001$). As in E10.5 embryos, no significant differences were seen upon comparing rostral wild type with rostral mutant compartments, or caudal wild type with caudal mutant compartments. Nevertheless, as suggested from the sections shown in Fig. 8A, cell densities were still lower in mutant, particularly in C1 and C2 and in the future AAA (arrows). The results are consistent with the fact that the derivatives of the rostral-most somites, which give rise to the basioccipital bone, the atlas, axis, and part of the dens axis (Muller and O'Rahilly, 2003), are more severely and more consistently affected phenotypically than the derivatives of more caudal cervical somites.

In contrast to the differences observed with BrdU labeling indices, no significant differences were seen with respect to cell death, regardless of whether TUNEL staining or activated caspase-3 labeling was performed to label apoptotic cells (Fig. 8B, showing histology for TUNEL and histology and quantitation for activated caspase-3 labeling). Hence, taken together, the results suggest that *Meox1*

Fig. 3. Formation of somites, sclerotome and cartilage in mutant embryos. (A, B) Sagittal sections through the first and second rostral somite at E9.5 (24 pairs of somites) show normal somite epithelialization and separation in both wild type (A) and *Meox1*$^{im/im}$ (B). (C–J) H&E stained sagittal sections through the cervical (C–H) and sacral (I, J) region of embryos of the indicated genotypes and ages. Note well-formed mesenchymal condensations in mid-sagittal section in wild type (C, arrow) but absence of such condensations in age-matched mutant (D). (n) notochord. (E, F) Parasagittal sections through cervical somites. Note clear separation of rostral (r) and caudal (c) portions of lateral sclerotome compartments and of dorsal root ganglia (arrow) in wild type (E). In mutant, the rostro-caudal separation of lateral sclerotomes is less well defined and the dorsal root ganglia are partially fused (F, arrow). At E12.5, wild type (G) shows well-formed vertebral anlagen and a prominent anlage of the AAA while in the mutant (H) the anterior arch is barely visible and shifted (arrow in H) towards the Bo. (I, J) Wild type also shows well-formed and equally spaced vertebral anlagen in the sacral region (I) while in the mutant (J), the anlagen are less well defined and unequally spaced (arrows). (K–Q) Alcian blue staining to reveal cartilage at E13.5 and 14.5 as indicated. (K, L) Sagittal vibratome sections of the cervical vertebra. In contrast to heterozygote (K), where the Bo is well separated from the At and its anterior arch (AAA), in homozygotes, the AAA cartilage forms a bridge with the Bo (L). (M, N) Vibratome sections show similar appearance of the nucleus pulposus of the future axio-cervical intervertebral disc in E14.5 wild type (M) and mutant (N). (O–Q) Parasagittal vibratome sections. In heterozygote (O), the cartilage of the Ex, the lateral arches of the At and Ax are well separated, while in a homozygote (P), the lateral arch of the Ax and cervical-3 (C3) vertebra are fused. (Q) Represents another homozygous mutant embryo showing a C3/4 cartilage fusion and a C7/Th1 (thoracic-1) cartilage bridge. Bar: 60 μm for A, B; 95 μm for C–F; 64 μm for G–J; 250 μm for K, L, O, P, Q; 38 μm for M, N.

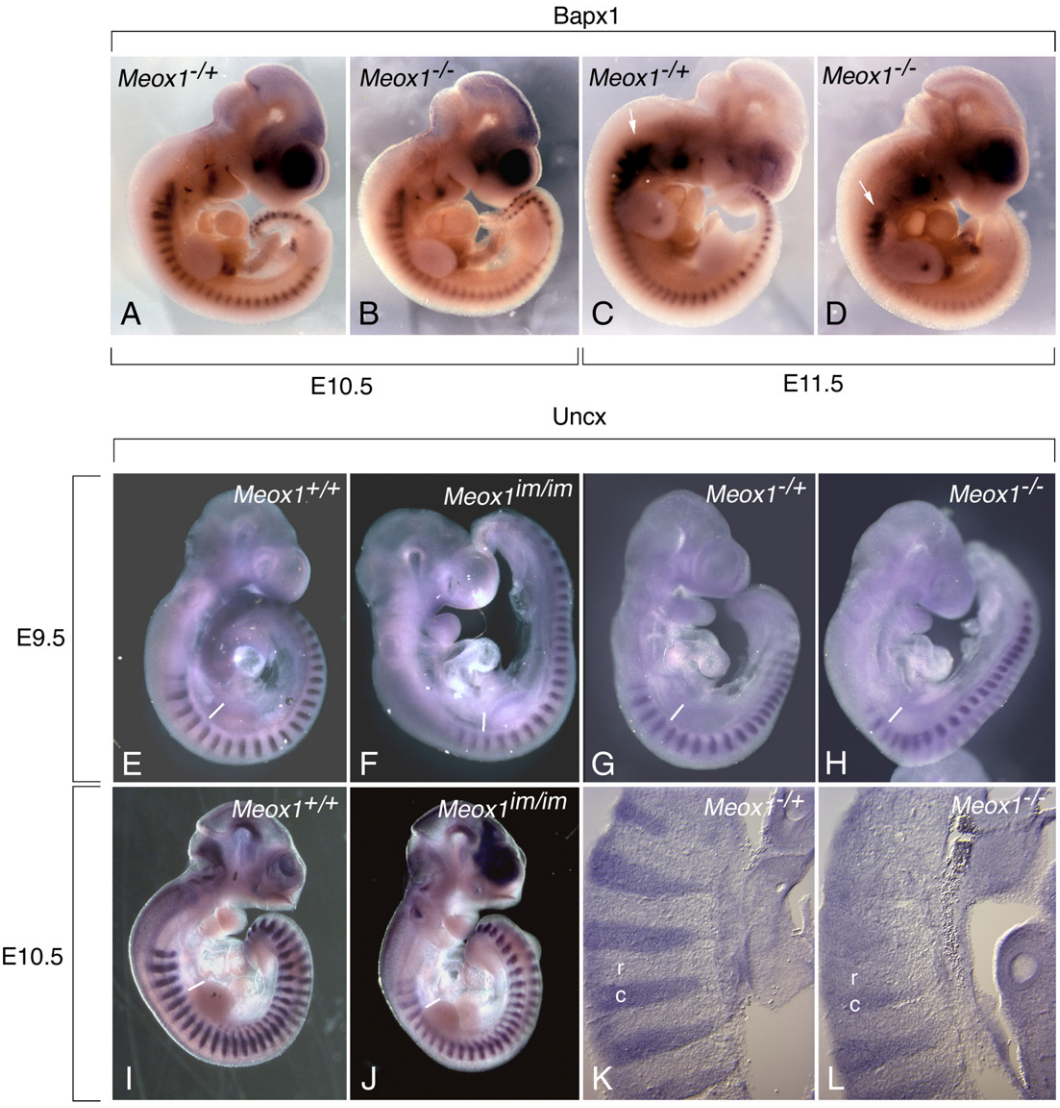

Fig. 5. Expression of markers altered by the absence of *Meox1*. Embryos of the indicated ages and genotypes were processed for whole mount in situ hybridization. (A–D) Labeling for Bapx1. Note that homozygous mutants show a slight reduction in staining along the entire axis at E10.5 and a more pronounced reduction at E11.5, in particular in rostral sclerotomes (arrows). (E–L) Labeling for Uncx. Note diminishment of staining in the rostral-most sclerotomes of the *Meox1* mutants. The rostral border of the limb bud is indicated (white line). (K, L) Sagittal vibratome sections through the rostral sclerotomes of *Meox1*$^{-/+}$ (K) and *Meox1*$^{-/-}$ (L). (r) rostral and (c) caudal sclerotome compartment.

affects sclerotome patterning by transiently affecting compartment-specific rates of cell proliferation.

Discussion

We show that two distinct null alleles of *Meox1*, each lacking a different essential portion of the gene, cause similar recessive phenotypes that affect the development of the axial skeleton but leave other somite derivatives and the appendicular skeleton intact. In contrast to the combined lack of both *Meox1* and *Meox2*, which severely disrupts somitic gene expression and somite formation, the lack of *Meox1* alone does not cause visible changes in the expression of many somitic genes and does not impair early somitogenesis. Indeed, alterations in expression were found only with three genes, *Tbx18*, *Bapx1*, and *Uncx*, with the latter showing abnormalities only in the developmentally older, rostral somites. This finding is consistent with the fact that the most prominent feature of the *Meox1* phenotype was a remodeling of the cranio-cervical joints which are derived from rostral somites.

Our observations provide multiple lines of evidence that the rostral abnormalities are due to developmental alterations in cell proliferation rates within the corresponding somites. First, at E10.5, changes in BrdU incorporation rates eliminate the characteristic intrasomitic rostro-caudal gradient and suggest an increase in rostral at the expense of caudal cell proliferation. Second, although the intrasomitic rostro-caudal differences in BrdU incorporation rates are restored at E12.5, they seem not to be able to fully compensate for the earlier abnormalities as cell densities are still abnormal, particularly in the rostral-most identifiable sclerotomes. Third, there are no genotype-dependent differences for markers of cell death. Fourth, the two *Meox1* mutations are both associated with a reduction in the expression levels of *Tbx18*, a gene whose null mutation has previously been shown to lead to changes in BrdU incorporation rates in rostral compared to caudal somite compartments. Fifth, *Bapx1*, which is required for the development of midline components of vertebrae and the somite-derived basioccipital and exoccipital bones of the chondrocranium (Tribioli and Lufkin, 1999), has also been reported to affect cell proliferation in the ventro-medial sclerotome (Akazawa et al., 2000). Sixth, MEOX1 protein is bound to conserved promoter sequences of *Bapx1* in vitro (Rodrigo et al., 2004) and *Tbx18* in vivo, suggesting that *Meox1* regulates these genes at least in part directly.

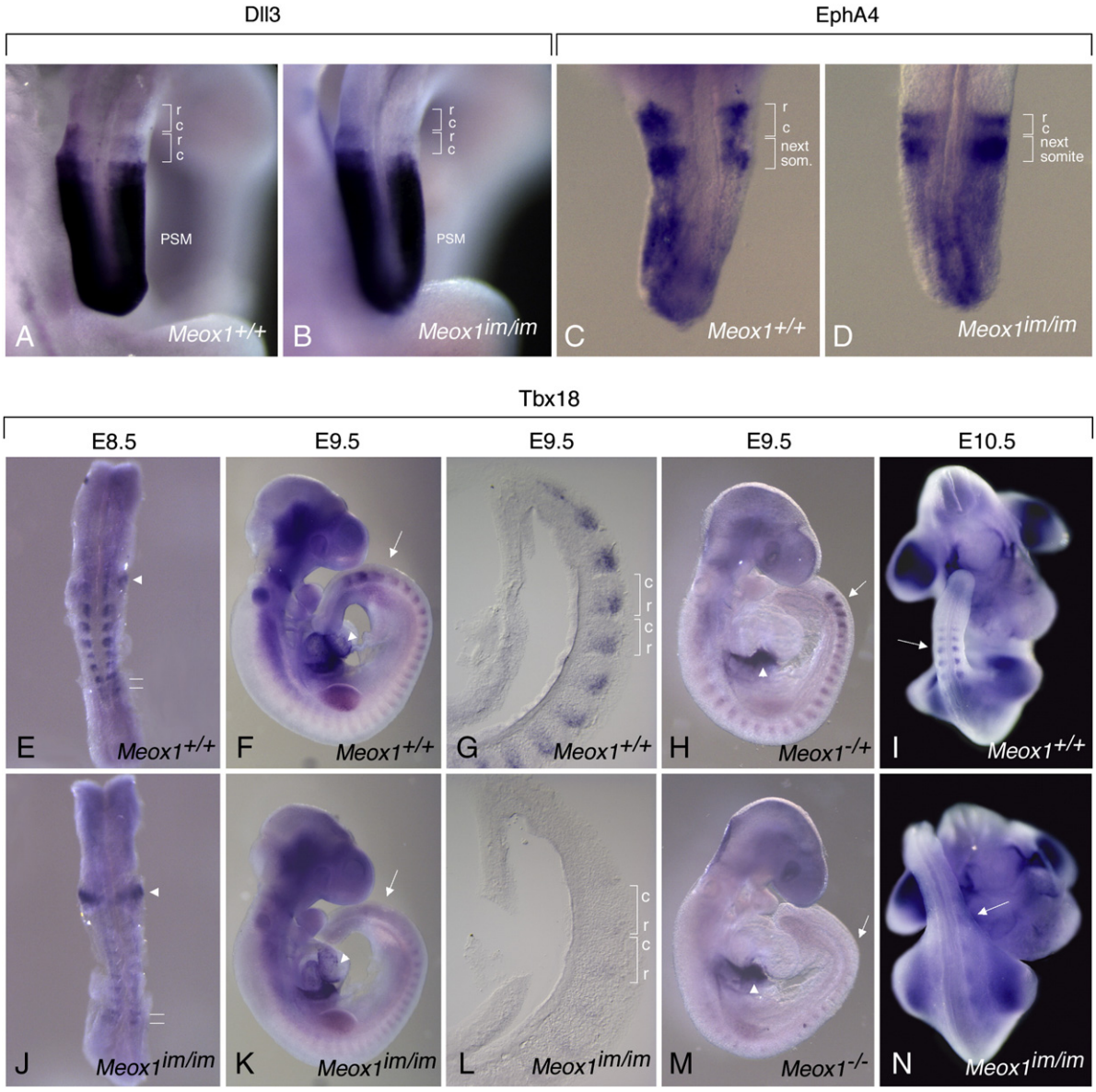

Fig. 6. Expression of markers specific for the rostral sclerotome compartment. (A, B) *Dll3* expression (E10.5) in wild type (A) and *Meox1*$^{im/im}$ (B) is similar in presomitic mesoderm (PSM) and newly formed somites. (C, D) Expression of *EphA4* in wild type (C) and *Meox1*$^{im/im}$ (D) is similar in the next forming somite and recently formed somite. (E–N) Expression of *Tbx18* in embryos of the indicated genotypes and ages. (E) At E8.5, a wild-type embryo shows two thin stripes in presomitic mesoderm (marked with horizontal lines) as well as staining in the rostral halves of somites. The arrowhead points to staining of the splanchnic mesoderm around the heart tube. (J) A corresponding *Meox1*$^{im/im}$ embryo shows similar label in presomitic mesoderm (horizontal lines) but reduced staining in somites. The splanchnic mesoderm around the heart tube, however, is strongly labeled (arrowhead). At all stages thereafter, *Tbx18* shows weaker somitic staining in mutant (K–N) compared with wild-type embryos (F–I) but normal staining in the proepicardium and in limb buds (compare F with K, H with M, arrowheads marking proepicardium). (G, L) Sagittal vibratome sections through the tails.

Nevertheless, despite the fact that mutations in *Meox1*, *Tbx18*, and *Bapx1* all affect BrdU incorporation rates, differences exist between the mutants with respect to the regulation of *Uncx* and the generation of more caudal phenotypes such as lumbar/sacral hemivertebrae and short, kinky tails. Previous results have shown, for instance, that in *Tbx18* mutants, *Uncx* expression is increased (Bussen et al., 2004), but in *Meox1* mutants, we find it to be decreased. Originally, it has been postulated that the increase in rostral-compartment *Uncx* expression in *Tbx18* mutants results from an immigration of caudal, *Uncx*-positive cells into the rostral compartment (Bussen et al., 2004). Such rostral migration has not been demonstrated, however, and so it was equally plausible that the increase in *Uncx* expression was due to a change in gene transcription directly in the rostral compartment. Indeed, the more recent finding that TBX18, in collaboration with Groucho, serves as a transcriptional repressor on a variety of promoters is compatible with a role of *Tbx18* in repressing *Uncx*, be it direct or indirect (Farin et al., 2007). But why, then, would a decrease in *Tbx18* expression in *Meox1* mutants lead to a *reduction* in *Uncx* expression, and this in both the rostral and caudal compartment, at least of rostral somites? We propose that this is so because *Meox1* is needed for the maintenance of *Uncx* expression, so that in the absence of *Meox1*, the lack of *Tbx18* can no longer de-repress *Uncx*. This view is supported by the finding that MEOX1 binds to conserved sequence elements in the putative *Uncx* upstream regulatory region, and it is compatible with the observation that in *Meox1* mutants, caudal derivatives such as pedicles, transverse processes, and proximal ribs are not expanded as seen in *Tbx18* mutants. The results suggest, therefore, that for the rostral somites, *Meox1*, *Tbx18* and *Uncx* are linked in regulatory crosstalks as schematically depicted in Fig. 9. This scheme is based on the previous observation that overexpression of the transcriptional repressor *Tbx18* (Farin et

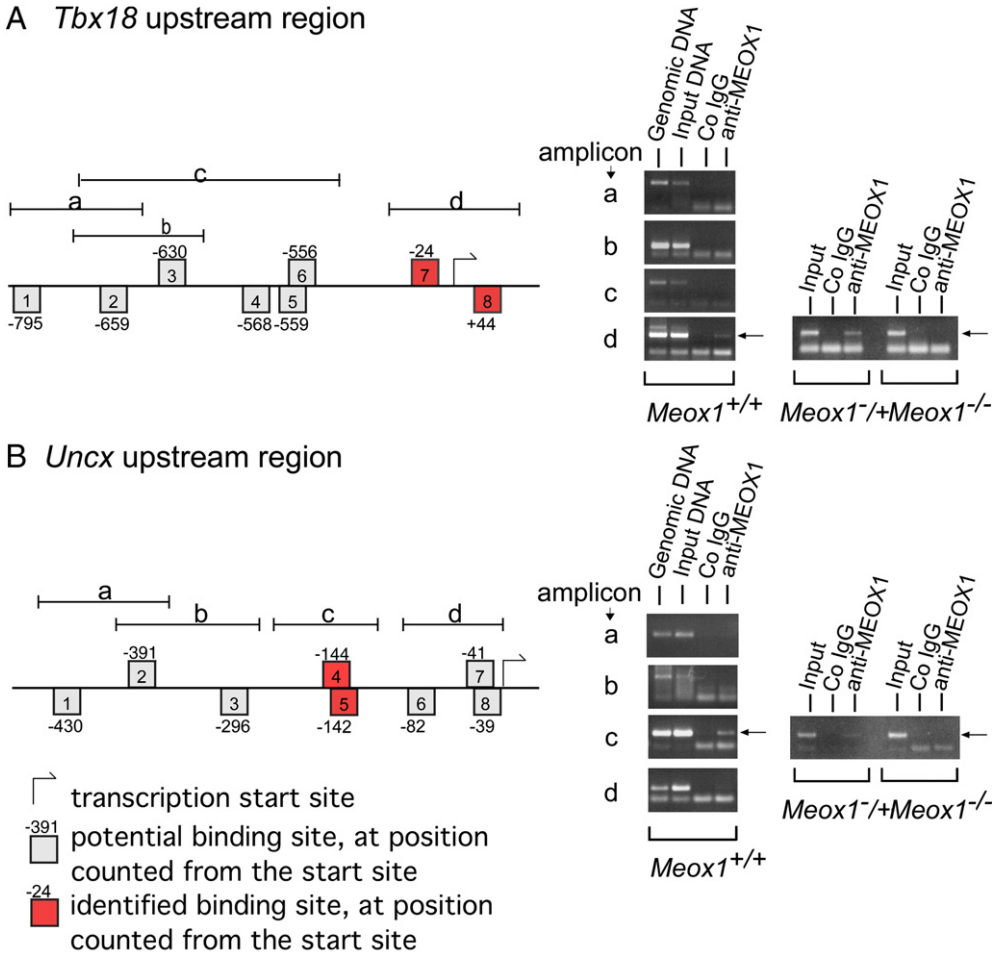

Fig. 7. In vivo binding of MEOX1 protein to promoter regions of *Tbx18* and *Uncx*. ChIP assays performed as indicated in Materials and methods. (A) *Tbx18* regulatory region. The left side shows the location of conserved potential homeodomain binding sites and the position of the respective amplicons. The middle panels show the bands resulting from the amplification of these amplicons from genomic DNA, DNA after shearing (input) and after immunoprecipitation with either control IgG or rabbit anti-MEOX1 antiserum. Only amplicon d shows MEOX1-specific amplification (arrow). The right panel shows the corresponding band for amplicon d in *Meox1*^{im}/+ and the absence of this band in *Meox1*$^{im/im}$. (B) Similar analysis for the *Uncx* regulatory region. Note that here, only amplicon c gave a MEOX1-specific signal in wild-type and *Meox1*^{im}/+, and no signal in *Meox1*$^{im/im}$.

al., 2007) results in downregulation of *Meox1* and *Uncx* (Bussen et al., 2004), and the results in this paper that *Tbx18* and *Uncx* are targets of *Meox1*. A crucial feature of the proposed regulatory loops is an initial rostro-caudal gradient of *Meox1* expression which is ultimately responsible for compartment-specific gene expression and the maintenance of sclerotome polarity. Nevertheless, how this gradient is established and maintained, how it integrates with other genes including *Bapx1*, and how these genes affect cell proliferation still need to be explored.

While the rostral abnormalities can thus be explained by the combined alterations in the expression of *Tbx18*, *Uncx*, and *Bapx1*, an explanation for the caudal phenotypes such as hemivertebrae and short, kinky tails may have to rest on the reduction in *Bapx1* expression alone. For instance, a reduction of *Tbx18* along the entire rostro-caudal axis would not in itself explain these phenotypes as the lack of *Tbx18* in *Tbx18*−/− mice, while leading to an overall shorter body axis similar to that observed with *Meox1* mutants, does not cause specific abnormalities in lumbar or tail vertebrae. Also, *Uncx* is unlikely to be involved as it remains normally expressed in more caudal somites. In contrast, *Bapx1* null mutants show hemivertebrae and kinky tails (Tribioli and Lufkin, 1999; Lettice et al., 1999; Akazawa et al., 2000). Nevertheless, it cannot be excluded that for the manifestation of the full skeletal phenotype, still other genes need to be affected, even if their alterations might not easily be seen by in situ hybridization.

Taken together, then, a picture emerges in which *Meox1* has a non-redundant function, not for the initial steps in somitogenesis including segmentation and polarization, but for the maintenance of sclerotome polarization over prolonged developmental time, as manifested mostly in the rostral somites. Given that in the *Meox1*/*Meox2* double mutants, somite polarization and sclerotome segmentation are entirely absent, we conclude that sclerotomal *Meox2* expression is sufficient to compensate for the lack of *Meox1* during the initial, but not the later, steps in somitogenesis. In fact, our previous analysis of double mutants has already hinted at functional dissimilarities between the two proteins in the sclerotome when we noted, in an analysis limited to skeletal stains of newborns, that the presence of just one copy of *Meox1* (and none of *Meox2*) leads to normal lumbar vertebrae, while the presence of one copy of *Meox2* (and none of *Meox1*) leads to split lumbar vertebrae (Mankoo et al., 2003). Although it is unclear whether this difference is due to a difference in sclerotomal expression levels between *Meox1* and *Meox2* or to intrinsic differences in the activities of the corresponding proteins, it indicates that *Meox1* and *Meox2* have functionally diverged following an ancient gene duplication even within still overlapping sclerotomal expression domains.

It is noteworthy that there are numerous human spondylocostal syndromes that share parts of the axial skeletal phenotype observed in *Meox1* mutant mice, including remodeling of the cranio-cervical joints, hemivertebrae, and vertebral fusions. Interestingly,

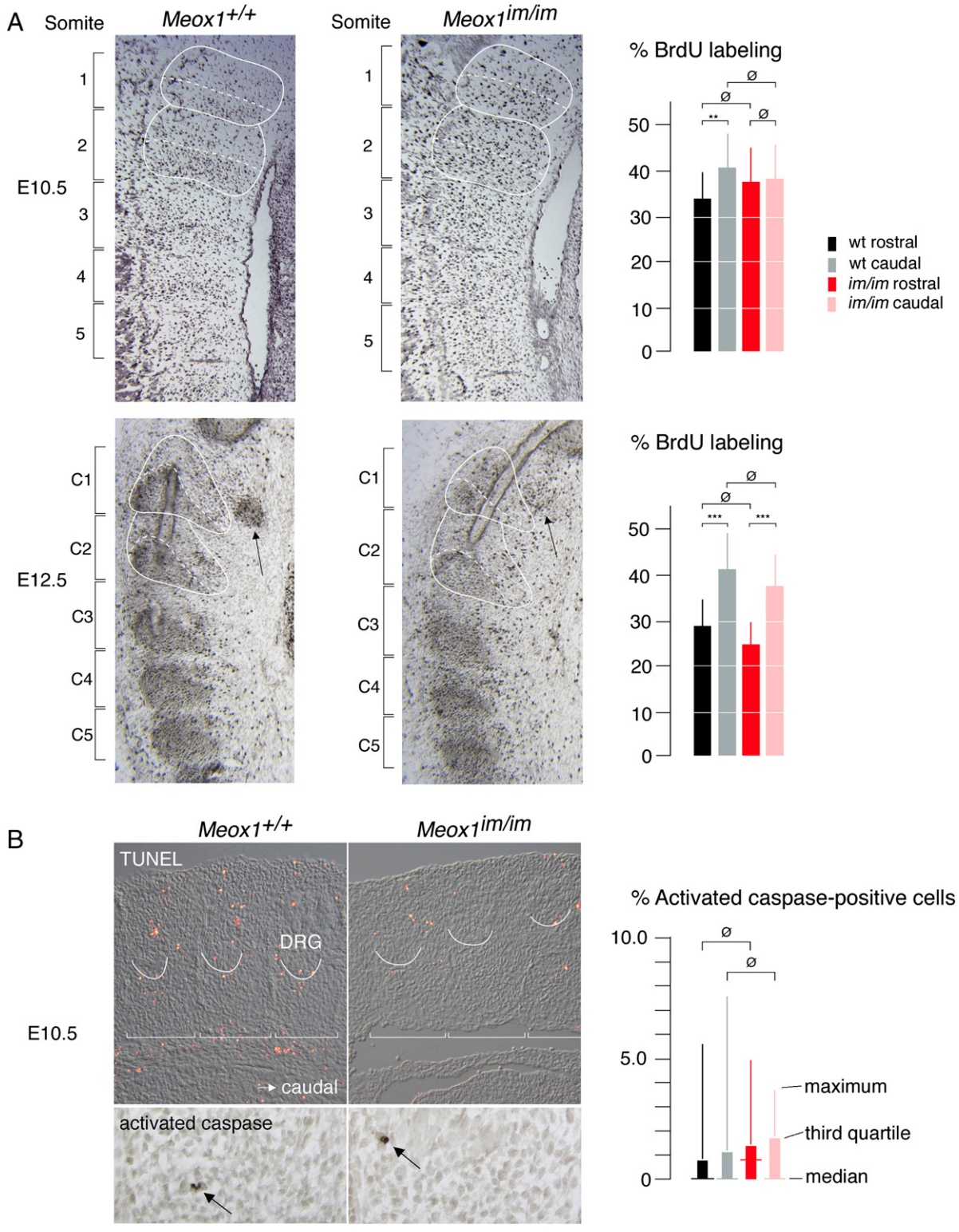

Fig. 8. Cell proliferation and cell death in wild-type and *Meox1*$^{im/im}$ sclerotomes. (A) BrdU incorporation. Left side shows representative areas selected for counting, with dashed lines marking the separation between rostral and caudal sclerotome. For E10.5, a total of 9332 cells were counted in wild type and 7401 in mutant (2 embryos/genotype, 4 sections total/somite 1–7). For E12.5, a total of 6950 cells were counted in wild type and 6405 cells in mutant (2 embryos/genotype, 3 sections total/somite C1–C2, 2 sections total/somite C3–7). For somite labeling and alignment, see text. Percent BrdU labeling (BrdU-positive cells/total cells × 100) is shown in the bar diagram on the right. Statistical analysis (Student's *t*-test) shows significant rostro-caudal differences for the combined values of somites 1–7 in wild type (**, $p = 0.013$) but not in *Meox1*$^{im/im}$ mutants (∅ , $p = 0.5$), and no significant differences if rostral or caudal labeling are compared between wild type and mutant (∅, $p > 0.34$). At E12.5, mutant somites still show reduced cell densities, particularly apparent in C1 and C2 and in the region of the anlage for the anterior arch of the atlas (arrows, area excluded from counting), but rostro-caudal differences in BrdU labeling indices are restored. Statistical analysis as for E10.5. (B) TUNEL and activated caspase-3 labeling at E10.5. For TUNEL labeling (red fluorescence), cervical somites are shown, with the white marks outlining tangential sections through dorsal root ganglia (DRG). Brackets mark sclerotome boundaries. Underneath are examples of activated caspase-3-positive cells in the lateral sclerotome. The box plots on the right are based on counts for somite 1–7 (three sections per somite, two embryos per genotype, with a total of 11,094 cells counted for wild type and 10,062 cells for mutant.). Median, third quartile and maximum percentage of positive cells (positive cells/total cells × 100) are shown. Differences were not statistically significant (Student's *t*-test).

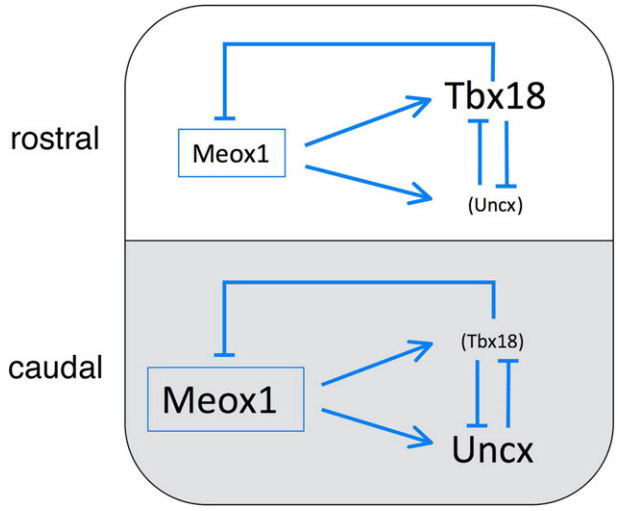

Fig. 9. Schematic representation of regulatory loops that link *Meox1*, *Tbx18*, and *Uncx* and operate in rostral somites. We propose that the regulatory loops are in principle similar in the rostral and caudal somite compartments but that initial rostro-caudal differences in the expression levels of *Meox1* (and *Meox2*, not shown) allow for high-level *Tbx18* expression in the rostral compartment, and high-level *Uncx* expression in the caudal compartment. Intersections of these pathways with *Bapx1* are not shown as little is known about potential crossregulations between *Tbx18*, *Uncx* and *Bapx1*. For details, see Discussion.

occipitalization of the atlas is associated with chromosomal abnormalities such as the deletion of the chromosomal region 22q11.2 that includes the *TBX1* gene (Ricchetti et al., 2004; Gholve et al., 2007). To our knowledge, however, none of these syndromes is an exact phenocopy of what we here describe in mice. Moreover, none of these syndromes has so far been precisely mapped to where *MEOX1* resides on human chromosome 17, *TBX18* on human chromosome 6, *UNCX* on human chromosome 7, or *BAPX1* on chromosome 4. Nevertheless, epigenetic dysregulation of *BAPX1* expression has been proposed to be associated with breakpoints of translocation involving chromosome 4 in patients with oculo-auriculo-vertebral spectrum (Fischer et al., 2006). From these observations we conclude that *MEOX1* and the molecular pathways, of which *MEOX1* is part, are still valid candidates for human abnormalities of the spine whose molecular causes have not yet been determined.

Acknowledgments

We thank Drs. B. Condie, B. Hogan, R. Hill and A. Kispert for reagents, Dr. E. Meier for invaluable help during the molecular characterization and Dr. Rudi Balling during the phenotypic characterization of the transgene insertion, and Drs. Lynn Hudson and Dubois-Dalcq for comments on the manuscript. We also thank Keith Rogers for preparing H&E sections, and the staff of the NINDS animal facility for excellent animal care. This work was supported in part by the Medical Research Council (BM and VP) and by the intramural research program of the NIH, NINDS.

Appendix A. Supplementary data

Supplementary data associated with this article can be found, in the online version, at doi:10.1016/j.ydbio.2009.06.006.

References

Akazawa, H., Komuro, I., Sugitani, Y., Yazaki, Y., Nagai, R., Noda, T., 2000. Targeted disruption of the homeobox transcription factor Bapx1 results in lethal skeletal dysplasia with asplenia and gastroduodenal malformation. Genes Cells 5, 499–513.

Bergemann, A.D., Cheng, H.J., Brambilla, R., Klein, R., Flanagan, J.G., 1995. ELF-2, a new member of the Eph ligand family, is segmentally expressed in mouse embryos in the region of the hindbrain and newly forming somites. Mol. Cell. Biol. 15, 4921–4929.

Bharti, K., Liu, W., Csermely, T., Bertuzzi, S., Arnheiter, H., 2008. Alternative promoter use in eye development: the complex role and regulation of the transcription factor MITF. Development 135, 1169–1178.

Burke, A.C., Nelson, C.E., Morgan, B.A., Tabin, C., 1995. Hox genes and the evolution of vertebrate axial morphology. Development 121, 333–346.

Bussen, M., Petry, M., Schuster-Gossler, K., Leitges, M., Gossler, A., Kispert, A., 2004. The T-box transcription factor Tbx18 maintains the separation of anterior and posterior somite compartments. Genes Dev. 18, 1209–1221.

Candia, A.F., Wright, C.V., 1996. Differential localization of Mox-1 and Mox-2 proteins indicates distinct roles during development. Int. J. Dev. Biol. 40, 1179–1184.

Candia, A.F., Hu, J., Crosby, J., Lalley, P.A., Noden, D., Nadeau, J.H., Wright, C.V., 1992. Mox-1 and Mox-2 define a novel homeobox gene subfamily and are differentially expressed during early mesodermal patterning in mouse embryos. Development 116, 1123–1136.

Condie, B.G., Capecchi, M.R., 1993. Mice homozygous for a targeted disruption of Hoxd-3 (Hox-4.1) exhibit anterior transformations of the first and second cervical vertebrae, the atlas and the axis. Development 119, 579–595.

Condie, B.G., Capecchi, M.R., 1994. Mice with targeted disruptions in the paralogous genes hoxa-3 and hoxd-3 reveal synergistic interactions. Nature 370, 304–307.

Dunwoodie, S.L., Henrique, D., Harrison, S.M., Beddington, R.S., 1997. Mouse Dll3: a novel divergent Delta gene which may complement the function of other Delta homologues during early pattern formation in the mouse embryo. Development 124, 3065–3076.

Farin, H.F., Bussen, M., Schmidt, M.K., Singh, M.K., Schuster-Gossler, K., Kispert, A., 2007. Transcriptional repression by the T-box proteins Tbx18 and Tbx15 depends on Groucho corepressors. J. Biol. Chem. 282, 25748–25759.

Fischer, S., Lüdecke, H.J., Wieczorek, D., Böhringer, S., Gillessen-Kaesbach, G., Horsthemke, B., 2006. Histone acetylation dependent allelic expression imbalance of BAPX1 in patients with the oculo-auriculo-vertebral spectrum. Hum. Mol. Genet. 15, 581–587.

Gholve, P.A., Hosalkar, H.S., Ricchetti, E.T., Pollock, A.N., Dormans, J.P., Drummond, D.S., 2007. Occipitalization of the atlas in children. Morphologic classification, associations, and clinical relevance. J. Bone Joint Surg., Am. 89, 571–578.

Gridley, T., 2006. The long and short of it: somite formation in mice. Dev. Dyn. 235, 2330–2336.

Haenig, B., Kispert, A., 2004. Analysis of TBX18 expression in chick embryos. Dev. Genes Evol. 214, 407–411.

Iida, K., Koseki, H., Kakinuma, H., Kato, N., Mizutani-Koseki, Y., Ohuchi, H., Yoshioka, H., Noji, S., Kawamura, K., Kataoka, Y., Ueno, F., Taniguchi, M., Yoshida, N., Sugiyama, T., Miura, N., 1997. Essential roles of the winged helix transcription factor MFH-1 in aortic arch patterning and skeletogenesis. Development 124, 4627–4638.

Kessel, M., Balling, R., Gruss, P., 1990. Variations of cervical vertebrae after expression of a Hox-1.1 transgene in mice. Cell 61, 301–308.

Kraus, F., Haenig, B., Kispert, A., 2001. Cloning and expression analysis of the mouse T-box gene Tbx18. Mech. Dev. 100, 83–86.

Kuijper, S., Beverdam, A., Kroon, C., Brouwer, A., Candille, S., Barsh, G., Meijlink, F., 2005. Genetics of shoulder girdle formation: roles of Tbx15 and aristaless-like genes. Development (Cambridge, England) 132, 1601–1610.

Leitges, M., Neidhardt, L., Haenig, B., Herrmann, B.G., Kispert, A., 2000. The paired homeobox gene Uncx4.1 specifies pedicles, transverse processes and proximal ribs of the vertebral column. Development 127, 2259–2267.

Lettice, L.A., Purdie, L.A., Carlson, G.J., Kilanowski, F., Dorin, J., Hill, R.E., 1999. The mouse bagpipe gene controls development of axial skeleton, skull, and spleen. Proc. Natl. Acad. Sci. U. S. A. 96, 9695–9700.

Mankoo, B.S., Collins, N.S., Ashby, P., Grigorieva, E., Pevny, L.H., Candia, A., Wright, C.V., Rigby, P.W., Pachnis, V., 1999. Mox2 is a component of the genetic hierarchy controlling limb muscle development. Nature 400, 69–73.

Mankoo, B.S., Skuntz, S., Harrigan, I., Grigorieva, E., Candia, A., Wright, C.V., Arnheiter, H., Pachnis, V., 2003. The concerted action of Meox homeobox genes is required upstream of genetic pathways essential for the formation, patterning and differentiation of somites. Development 130, 4655–4664.

Mansouri, A., Voss, A.K., Thomas, T., Yokota, Y., Gruss, P., 2000. Uncx4.1 is required for the formation of the pedicles and proximal ribs and acts upstream of Pax9. Development 127, 2251–2258.

Muller, F., O'Rahilly, R., 2003. Segmentation in staged human embryos: the occipitocervical region revisited. J. Anat. 203, 297–315.

Nakajima, Y., Morimoto, M., Takahashi, Y., Koseki, H., Saga, Y., 2006. Identification of Epha4 enhancer required for segmental expression and the regulation by Mesp2. Development 133, 2517–2525.

Nakayama, A., Nguyen, M.T., Chen, C.C., Opdecamp, K., Hodgkinson, C.A., Arnheiter, H., 1998. Mutations in microphthalmia, the mouse homolog of the human deafness gene MITF, affect neuroepithelial and neural crest-derived melanocytes differently. Mech. Dev. 70, 155–166.

Ricchetti, E.T., States, L., Hosalkar, H.S., Tamai, J., Maisenbacher, M., McDonald-McGinn, D.M., Zackai, E.H., Drummond, D.S., 2004. Radiographic study of the upper cervical spine in the 22q11.2 deletion syndrome. J. Bone Joint Surg., Am. 86-A, 1751–1760.

Rodrigo, I., Bovolenta, P., Mankoo, B.S., Imai, K., 2004. Meox homeodomain proteins are required for Bapx1 expression in the sclerotome and activate its transcription by direct binding to its promoter. Mol. Cell. Biol. 24, 2757–2766.

Singh, M.K., Petry, M., Haenig, B., Lescher, B., Leitges, M., Kispert, A., 2005. The T-box transcription factor Tbx15 is required for skeletal development. Mech. Dev. 122, 131–144.

Sporle, R., Schughart, K., 1997. System to identify individual somites and their derivatives in the developing mouse embryo. Dev. Dyn. 210, 216–226.
Takahashi, Y., Sato, Y., 2008. Somitogenesis as a model to study the formation of morphological boundaries and cell epithelialization. Dev. Growth Differ 50 (Suppl 1), S149–S155.
Tanaka, M., Tickle, C., 2004. Tbx18 and boundary formation in chick somite and wing development. Dev. Biol. 268, 470–480.
Tribioli, C., Lufkin, T., 1999. The murine Bapx1 homeobox gene plays a critical role in embryonic development of the axial skeleton and spleen. Development 126, 5699–5711.
Wilm, B., Dahl, E., Peters, H., Balling, R., Imai, K., 1998. Targeted disruption of Pax1 defines its null phenotype and proves haploinsufficiency. Proc. Natl. Acad. Sci. U. S. A. 95, 8692–8697.
Winnier, G.E., Hargett, L., Hogan, B.L., 1997. The winged helix transcription factor MFH1 is required for proliferation and patterning of paraxial mesoderm in the mouse embryo. Genes Dev. 11, 926–940.